PERGAMON

Quaternary Science Reviews 22 (2003) 953–959

QG QSR

High-resolution chronologies for loess: comparing AMS ^{14}C and optical dating results

A. Lang[a,*], C. Hatté[b], D.-D. Rousseau[c,d], P. Antoine[e], M. Fontugne[b], L. Zöller[f], U. Hambach[f]

[a] *Fysische en Regionale Geografie, K.U. Leuven, Redingenstraat 16, B-3000 Belgium*
[b] *Laboratoire des Sciences du Climat et de l'Environnement, UMR1572 CEA/CNRS, Gif-sur-Yvette cedex F-91198, France*
[c] *Paléoenvironnement et Palynologie, Institut des Sciences de l'Évolution, UMR 5554-CNRS, Université Montpellier II, Place E. Bataillon, Montpellier cedex 5 F-34095, France*
[d] *Lamont-Doherty Earth Observatory of Columbia University, Palisades, NY 10964, USA*
[e] *Laboratoire de Géographie Physique-CNRS, UMR CNRS 8591, 1 Place Aristide Briand, Meudon cedex 92 195, France*
[f] *Lehrstuhl Geomorphologie, Universität Bayreuth, Bayreuth D-95440, Germany*

Abstract

The Nußloch loess section in South West Germany is famous in Central Europe for its thick deposits from the Last Glacial Maximum. It has therefore been intensively studied during the past few years and offers an excellent opportunity to compare the performance of different dating techniques covering the period 15–45 ka.

Here we present results from optical and AMS ^{14}C dating. The silt-sized polymineral fraction of the clastic sediments and a multiple-aliquot approach was used for IR-OSL dating. ^{14}C dating was carried out on organic macro-remnants and humin fractions extracted from the sediments.

With the exception of samples taken from the uppermost 1.5 m of the section, IR-OSL and calibrated ^{14}C-AMS ages are consistent over the entire period. The inconsistencies in the upper meters are thought to be due to disturbances during soil formation in the Holocene. The good agreement obtained on the remaining sequence demonstrates the high accuracy of both methods when studying loess sections: for the IR-OSL ages no significant age underestimations are obvious.

The results clearly document that accurate chronologies can be developed for such continental sedimentary sequences. This gives access to archives that can now be studied with a high temporal resolution and allows the establishment of new paleoclimatic proxies for the study of terrestrial responses to past climatic changes.

1. Introduction

Robust records of past climate changes are required for evaluation and prediction of human impacts on future environments and climates. Traditional sources of paleoclimatic information with long temporal coverage and high resolution are ice cores and deep-sea records. However, it is continental records that yield information on the response of human environments to climate changes. But establishing precise and accurate chronologies for continental sedimentary sequences remains a key problem. The major archives that are used for reconstructing continental paleoclimates over the last glacial–interglacial cycle are lake deposits and loess sequences. Timeframes for limnic sequences were established mainly based on ^{14}C dating of macroscopic organic remnants. Chronologies of loess sequences were established mainly based on luminescence dating and only a few ^{14}C dates were available from very rare macroscopic organic remnants. Thus, in most cases, chronologies established for loess deposits were rather coarse. Due to the high sedimentation rates, that in some cases reach more than 1 cm in 10 years, these sedimentary sequences in principle would allow one to study climates during glacial periods at a very high temporal resolution. Such is necessary to understand how continental climate responded to changes in oceanic circulation.

Based on the pioneering work of Huntley et al. (1985) and Hütt et al. (1988) optically stimulated luminescence (OSL or optical) dating techniques provide the

*Corresponding author. Tel.: +32-16-326406; fax.: +32-16-326400.
E-mail address: andreas.lang@geo.kuleuven.ac.be (A. Lang).

0277-3791/03/$ - see front matter
doi:10.1016/S0277-3791(03)00035-0

possibility of dating a mineral grain's last exposure to daylight and thus its deposition. During the last few years the applicability of optical dating has been shown for various sedimentary environments (Roberts et al., in press; Stokes et al., in press; Wallinga and Lang, in press). Furthermore, AMS techniques provide now a new way to establish reliable and fine chronologies by ^{14}C dating of sparse but near ubiquitous organic matter (Hatté et al., 2001a).

The aim of this study is to test the performance of optical and ^{14}C dating as a step towards establishing a solid backbone for high-resolution chrono-stratigraphies of loess. Infrared-stimulated luminescence (IR-OSL) dating of polymineral silt and ^{14}C dating of loess organic matter are used for establishing a chronological framework for loess deposits from Nußloch, Germany.

2. Materials

The Nußloch loess sequence is located in the right uplifted block of the Upper Rhine graben (49.3°N–8.8°E; Fig. 1). The section has been intensively studied since the 1970s (Zöller et al., 1988). Antoine et al. (2001) describe in detail sediments and soils at the section. The sub-sequence representing the last interglacial/glacial climatic cycle is more than 18 m thick. It starts with a fossil B_t horizon from a truncated last interglacial soil that is overlain by three distinct horizons consisting of clayey and humic material and representing the Lower Würmian. The Lower Pleniglacial is represented by ca. 3 m of compact sandy loess in which tundra gley soils are preserved. The overlaying 3 m of typical calcareous loess originates from the Middle Würmian period and is bordered by two brown clayey horizons of arctic brown soils. A hiatus is present in the main loess section at 13.2 m depth. The upper 11.3 m typical calcareous loess was deposited during the Late Würmian. At the top 0.7 m thick truncated Holocene soil is preserved.

Carbonate contents throughout the sub-section range between 0% in the last interglacial B_t and 30–40% in the loess sediments. Contents of organic carbon are very low, usually below 0.1%, except for the paleosols at around 8, 10 and 14 m, where organic carbon contents reach 0.3%.

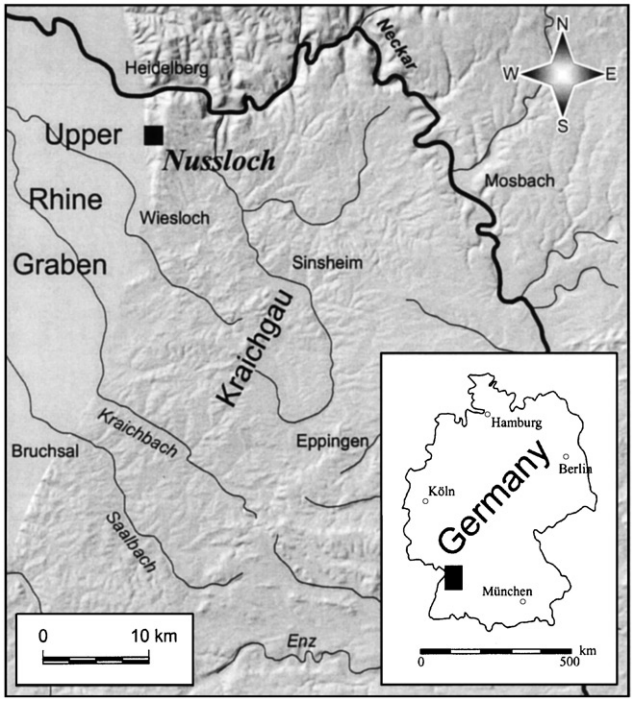

Fig. 1. Location of the sampling site.

3. Methods

3.1. Luminescence dating

For optical dating, polymineral fine-grain fractions (4–11 μm) were extracted from the sediments. The procedures used for sample preparation, luminescence measurements, equivalent dose (D_E) and dose-rate determination, and age calculation are reported in detail by Lang et al. (1996). OSL was detected in the 390–450 nm wavelength range (filters: BG 39, 2 BG 3 and GG 400, 3 mm each; Krbetschek and Rieser, 1995) and stimulated using 60 s IR stimulation (880Δ80 nm, TEMT diodes delivering ~40 mW/cm^2). Multiple-aliquot, additive-dose protocols were applied. Following Felix and Singhvi (1997), additive growth curves were constructed using 10 'natural' discs and six groups of artificially dosed discs (five each). A $^{90}Sr/^{90}Y$ β-source (dose rate ~10 Gy/min) was used for artificial dosing. Storage of 1 month at room temperature after irradiation was applied to all samples before measurement. Preheating at 220°C for 5 min was applied. The integral signal 0–40 s was used for IR-OSL D_E determinations after subtracting the mean IR-OSL intensity of the interval 50–60 s (subtraction technique following Aitken and Xie, 1992). Fading tests were carried out using an additional set of natural and maximum dosed sub-samples, which have been irradiated and preheated contemporary to the discs used for D_E determination, but were measured after 3 months of storage. The ratios of 'natural' intensities to 'artificially irradiated' intensities for the first and second measurements are compared to check for fading. Dose rates were calculated using a combination of α-counting, β-counting and low-level γ-spectrometry (Lang et al., 1996).

Table 1
Optical dating results: Sample code, sampling depth, water content (Δ), α-efficiency factor (a-value), U-, Th- and K-concentrations determined using low level γ-spectrometry; cosmic dose rate (dD_{cosmic}/dt), total dose rate (dD/dt), equivalent dose (D_E) and optical age are listed (in none of the samples significant radioactive disequilibrium was present)

Sample	Depth (m)	Δ[a]	a-value	U[b] (μg/g)	Th (μg/g)	K (%)	dD_{cosmic}/dt (Gy/ka)	dD/dt (Gy/ka)	D_E[c] (Gy)	Age (ka)
HDS 234	1.2	1.2±0.1	0.09±0.01	3.22±0.14	7.95±0.30	1.22±0.11	0.19	3.13±0.21	62.0±5.4	19.8±2.2
HDS 235	2.1	1.2±0.1	0.08±0.01	3.22±0.19	7.90±0.52	1.14±0.08	0.18	2.95±0.12	61.5±4.6	20.8±1.8
HDS 236	2.8	1.2±0.1	0.08±0.01	3.34±0.15	9.26±0.33	1.27±0.11	0.16	3.27±0.23	59.5±11.4	18.2±3.7
HDS 237	3.1	1.2±0.1	0.08±0.01	3.77±0.23	9.82±0.60	1.37±0.09	0.18	3.42±0.24	66.6±6.4	19.5±2.3
HDS 238	3.4	1.2±0.1	0.08±0.01	3.59±0.16	9.16±0.35	1.27±0.12	0.14	3.33±0.22	64.0±4.0	19.2±1.7
HDS 239	4.2	1.2±0.1	0.07±0.01	3.60±0.12	9.43±0.17	1.26±0.09	0.16	3.22±0.22	65.5±1.6	20.3±1.5
HDS 240	4.8	1.2±0.1	0.07±0.01	3.65±0.17	9.61±0.38	1.37±0.13	0.15	3.25±0.22	74.5±7.8	22.9±2.9
HDS 241	5.7	1.2±0.1	0.07±0.01	3.50±0.12	9.05±0.17	1.25±0.09	0.15	3.39±0.19	68.6±7.3	20.2±2.4
HDS 242	6.4	1.2±0.1	0.07±0.01	3.23±0.14	7.88±0.27	1.06±0.09	0.14	2.82±0.20	59.9±2.9	21.2±1.8
HDS 243	7.6	1.2±0.1	0.06±0.01	3.32±0.11	8.83±0.16	1.17±0.08	0.13	2.90±0.20	56.8±5.7	19.6±2.4
HDS 244	8.6	1.2±0.1	0.07±0.01	3.62±0.13	9.21±0.18	1.20±0.08	0.12	3.06±0.22	79.3±11.0	26.0±4.0
HDS 245	9.1	1.2±0.1	0.07±0.01	2.97±0.14	7.69±0.30	0.96±0.09	0.12	2.76±0.20	68.5±10.2	24.8±4.1
HDS 246	9.4	1.2±0.1	0.05±0.01	3.40±0.11	8.72±0.16	1.16±0.08	0.11	2.71±0.22	62.7±3.9	23.2±2.4
HDS 233	9.65	1.2±0.1	0.09±0.02	4.01±0.43	9.62±0.63	1.19±0.08	0.11	3.38±0.32	84.0±14.0	24.8±4.7
HDS 247	11.0	1.2±0.1	0.09±0.01	3.30±0.12	8.89±0.19	1.04±0.08	0.11	2.91±0.22	85.9±8.6	29.5±3.7
HDS 248	11.85	1.2±0.1	0.08±0.01	3.19±0.15	9.61±0.36	1.25±0.12	0.10	3.18±0.25	108.2±5.6	34.0±3.2
HDS 249	12.2	1.2±0.1	0.09±0.01	3.37±0.15	7.52±0.29	1.02±0.10	0.10	3.00±0.22	99.2±14.0	33.1±5.2
HDS 250	12.7	1.2±0.1	0.08±0.01	3.12±0.11	8.53±0.17	1.02±0.07	0.10	2.89±0.20	89.7±10.1	31.1±4.1
HDS 232	15.45	1.2±0.1	0.07±0.01	3.14±0.13	8.34±0.28	1.12±0.10	0.10	2.78±0.21	155±33	55.7±12.6
HDS 230	18.55	1.2±0.1	0.11±0.01	3.78±0.21	12.73±0.60	1.83±0.12	0.09	4.51±0.32	277±40	61.3±9.9
HDS 231	19.55	1.2±0.1	0.07±0.02	3.17±0.19	8.87±0.56	1.34±0.09	0.09	2.99±0.26	365±43	122.0±17.8

[a] Water content (ratio of wet sample weight to dry sample weight, Δ) was set to 1.2±0.1.
[b] U-content is calculated as mean equivalent U-concentration calculated from ^{214}Bi and ^{214}Pb activities, determined using low-level γ-spectrometry and the 295, 352 and 609 keV lines, and applying error weighting.
[c] D_E was determined using the subtraction technique (Aitken and Xie, 1992) and the integral signal from 0 to 40 s stimulation time.

3.2. ^{14}C dating

All ^{14}C analyses were carried out at the ^{14}C Laboratory at the Laboratoire des Sciences du Climat et de l'Environnement (LSCE), using β-counting in the underground laboratory of Modane (sample referenced Gif/LSM) and AMS (samples referenced GifA) facilities of Gif-sur-Yvette Tandétron (UMS, 2004).

All available macroscopic organic remnants were collected, i.e. gastropod shells at 1.6 m depth, and wood and bone fragments from a second outcrop corresponding to the stratigraphic position at 13.2–13.4 m depth (Antoine et al., 2001). They were treated using chemical preparation techniques routinely used in the radiocarbon laboratory of LSCE and measured through β-counting or AMS facilities (Hatté et al., 2001a). In addition, ca. 2 g of loess were sampled in 5–10 cm intervals from the upper part of the sequence and dried at 50°C, within 2 days after collection. From all samples root remains were discarded by handpicking and sieving to <200 μm. The remaining fraction was homogenised. The protocols used for extraction of the humin fraction and for AMS target preparation are reported in detail by Hatté et al. (2001a).

^{14}C ages are expressed in years B.P. and reflect normalisation to δ^{13}C. Ages younger than 18 ka B.P. were calibrated using the Stuiver and Reimer calibration (1993) (a cal. B.P.) and ages older than 18 ka B.P. were corrected according to Kitagawa and van der Plicht (1998) (a cor. B.P.).

4. Results and discussion

Analytical data and results from IR-OSL dating are listed in Table 1. In none of the samples radioactive disequilibrium was present. None of the samples showed significant anomalous fading after 3 months of storage. Examples of IR-OSL measurements and D_E determinations can be seen in Fig. 2. The reproducibility of the IR-OSL measurements was excellent. All samples investigated by IR-OSL showed shine-plateaux (constant D_E for all shine-times) after applying the subtraction technique (Aitken and Xie, 1992), which is a necessity for IR-OSL dating using multiple-aliquot, additive-dose protocols (Lang and Wagner, 1997).

IR-OSL ages and ^{14}C ages are listed according to the depth of sampling in Table 2 and plotted in Fig. 3. Overall the accordance of the data is striking. Ages range from 19 ka at the top of the section to 122 ka at the bottom. Within error limits, ages are in stratigraphic order and with few exceptions IR-OSL ages and ^{14}C

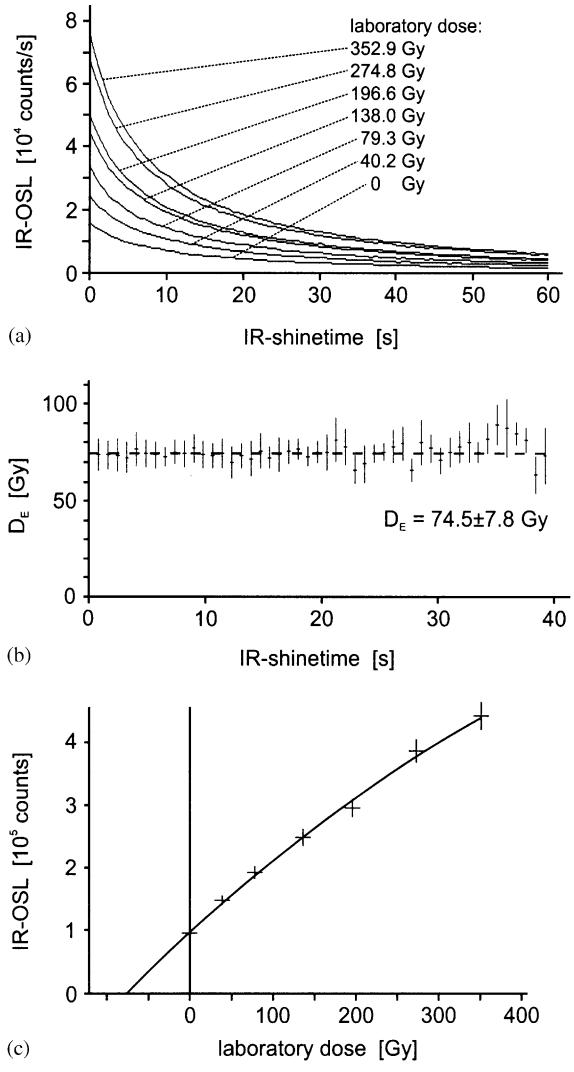

Fig. 2. (a) IR-shine down curves of sample HDS 240. Each curve represents the mean of 5–10 measurements. Artificial doses are indicated. (b) D_E values obtained for different shine-times for sample HDS 240 after applying the subtraction technique. The broken line marks the D_E value of 74.5 Gy (Fig. 2c). (c) Growth curve for sample HDS 240 using the integral signal from 0 to 40 s. The calculated D_E is 74.5 ± 7.8 Gy.

ages agree. IR-OSL ages are less precise because the uncertainty stated for the IR-OSL ages includes random errors and all quantifiable systematic errors, whereas for ^{14}C ages only random errors have been taken into account.

The results give confidence in the applied IR-OSL dating procedures: neither age overestimations nor underestimations are obvious.

The youngest IR-OSL ages agree well with the regional Quaternary history. Loess deposition in the area occurred until about 15 ka ago (Antoine et al., 1999; Frechen, 1999). The upper 1.5 m or so of sediments deposited at the site have been eroded; thus the youngest sediments could not be sampled. When looking at the radiocarbon results the two uppermost dates obtained on organic matter at 0.8 and 1.3 m depth should be taken cautiously. Strong soil formation took place during the Holocene temperate climatic conditions and a thick soil developed (more than 1.5 m of soil is missing in the studied section). Due to root and bacterial action, recent organic substances were found down to ca. 1.5 m depth. The ^{14}C date obtained on gastropod shells from 1.6 m depth should also be taken cautiously. It is well known that fossil carbonate can be incorporated by gastropods (e.g. Goodfriend and Hood, 1983). Such may result in an age overestimation of up to 2000 years.

Also, IR-OSL ages obtained on the oldest part of the section agree well with independent age estimates. For the loess underlying the last interglacial soil a reasonable age of 122.0 ± 17.8 ka is obtained. For the time-span 20–40 ka, for which results from both methods are available, IR-OSL and ^{14}C data agree. Indeed, unlike Holocene, the cold and often more arid glacial times are not favourable to intense biologic activity and only open types of vegetation existed. Thus also root action was limited. Furthermore, loess accumulation rates were very high and did not allow strong pedogenesis. Consequently, the organic matter turnover was negligible and radiocarbon ages closely reflect the time of loess deposition. This explains the good agreement existing between ^{14}C ages on organic matter, resulting from plant degradation, and IR-OSL ages, mirroring the time of loess deposition. Nevertheless, some ^{14}C age inversions occur in samples taken from weakly developed gley soil horizons (tundra-gleys, samples GifA-98366, GifA-99019, GifA-99021, and GifA-98366). Here iron concentrations are higher than 2% (Antoine et al., 2001) and free iron occurs as Fe^{2+} ions. The most probable explanation may be a contamination during laboratory treatments. Especially during alkali treatment dissolved atmospheric CO_2 is incorporated in the sample structure as ferrous carbonate and cannot be removed by further acid treatment. An alternative is proposed in Hatté et al. (2001b), but due to the small amount of material, it could not be applied here. Refining the chemical treatment for samples from gley horizons may improve the results. Taking out these unreliable ^{14}C ages performed on gley, ^{14}C chronology fits obviously with the IR-OSL one.

IR-OSL is derived from feldspar grains within the polymineral sample extracts and thus should be subject to anomalous fading (e.g. Huntley and Lamothe, 2001). However, when comparing the IR-OSL ages with the corrected ^{14}C ages, fading seems to be not significant. This could be due to (I) feldspars from this locality might not exhibit anomalous fading, (II) the preheat, storage and wavelength selection limit the IR-OSL analysis basically to a non-fading component, or (III) the studied timeframe is too short to allow for

Table 2
Dating results: OSL sample No., OSL age, depth of sampling, conventional ^{14}C-age, calibrated ^{14}C-age interval (for ages <18 ka) or corrected ^{14}C-age interval (for ages <18 ka), and ^{14}C sample No. are listed

Depth (m)	OSL sample No.	OSL Age (1σ) (a)	^{14}C sample No.	Conventional ^{14}C age (1σ) (a)[a]	Calibrated or corrected ^{14}C age (2σ) (a)[a]
0.8			GifA-99010[b]	3050±70	3061–3387
1.2	HDS 234	19 800±2200			
1.3			GifA-99011[b]	3580±70	3688–4000
1.6			GifA-96221[c]	15 260±110	18 162–18 702
1.6			GifA-96244[d]	12 880±110	14 777–15 777
2.1	HDS 235	20 800±1800			
2.2			GifA-99012[b]	12 670±100	14 497–15 316
2.8	HDS 236	18 200±3700			
3.0			GifA-99013[b]	18 170±180	21 131–22 258
3.1	HDS 237	19 500±2300			
3.4	HDS 238	19 200±1700			
3.8			GifA-99014[b]	17 250±140	19 944–20 996
4.2	HDS 239	20 300±1500			
4.8	HDS 240	22 900±2900			
5.0			GifA-99015[b]	19 590±220	21 950–23 900
5.7	HDS 241	20 200±2400			
5.8			GifA-98366[b]	14 270±120	16 780–17 420
6.3			GifA-99016[b]	18 350±160	21 404–22 433
6.4	HDS 242	21 200±1800			
7.0			GifA-99017[b]	19 100±180	21 400–23 700
7.5			GifA-99018[b]	22 100±220	24 400–26 400
7.6	HDS 243	19 600±2400			
7.8			GifA-99019[b]	15 490±140	18 084–18 711
8.6	HDS 244	26 000±4000			
9.0			GifA-98367[b]	24 020±250	25 900–29 100
9.1	HDS 245	24 800±4100			
9.4	HDS 246	23 200±2400			
9.7	HDS 233	24 800±4700			
9.7			GifA-99020[b]	21 340±190	24 000–25 600
10.3			GifA-99021[b]	11 700±120	13 340–13 989
11.0	HDS 247	29 500±3700			
11.1			GifA-99022[b]	25 700±270	27 200–31 300
11.8			GifA-99023[b]	26 000±310	28 400–31 400
11.9	HDS 248	34 000±3200			
12.2	HDS 249	33 100±5200			
12.7	HDS 250	31 100±4100			
12.8			GifA-99024[b]	26 670±300	28 800–31 400
13.2			GIF/LSM-10442[b]	31 800±400	32 025–35 575
13.2			GifA-97291[e]	32 270±500	35 475–39 325
13.2			GifA-97292[e]	32 180±470	35 525–39 275
13.2			GifA-97294[e]	32 800±510	35 475–39 325
13.3			GifA-97328[f]	35 800±1200	34 700–40 500
13.4			GifA-99025[b]	42 100±1200	41 100–47 000
13.9			GifA-98366[b]	31 400±440	32 500–36 200
15.5	HDS 232	55 700±12 600			
18.6	HDS 230	61 300±9900			
19.6	HDS 231	122 000±17 800			

[a] Adopted from Hatté et al. (2001a).
[b] Loess organic matter.
[c] Gastropod carbonate shells.
[d] Gastropod conchioline.
[e] Wood.
[f] Bone.

significant effects. Because sediments sampled from the region that should have a similar provenance showed fading (Lang and Wagner, 1997) and significant fading has been reported over much shorter time spans from other regions (Lamothe and Auclair, 1997), at the moment the most probable conclusion is that the

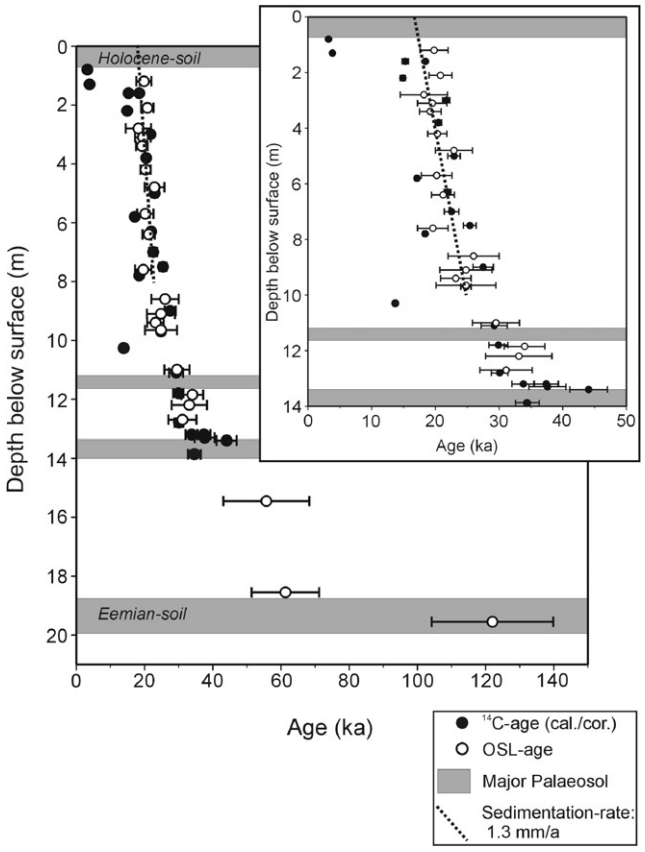

Fig. 3. Age versus depth plot. ^{14}C and optical ages are plotted according to the depth of sampling. Additionally, the location of major soils is indicated and a line is drawn pointing to a sedimentation rate of 1.3 mm a^{-1}. An enlargement of the upper 14 m is given in the inset.

applied protocol makes use of a rather stable component only.

Based on the dating results a mean deposition rate of 1.3 mm/year can be calculated for the upper 10 m of deposits (Fig. 3). However, in the loess from the Upper Pleniglacial seven tundra-gley horizons occur which represent halts in aeolian sedimentation. Thus, the sedimentation during this period was clearly not constant and maximum rates were much higher than the mean. Indeed, within the finely laminated facies of the Upper Pleniglacial (between about 3.5 and 10 m; Antoine et al., 2001) numerous sandy beds indicate single, up to 8 mm thick, deposition events.

This shows the potential high resolution that can be obtained for paleoclimatic reconstructions based on loess from the LGM.

5. Conclusions

The good agreement between IR-OSL and ^{14}C-AMS dating results demonstrates the high accuracy that can be obtained when studying loess sections. Such robust chronologies can then be used to develop high-resolution chrono-stratigraphies (Antoine et al., 2001). In combination with climate proxy records such as grain-size indices (Rousseau et al., 2002) and $\delta^{13}C$ variations (Hatté et al., 2001c) the Late Pleistocene paleoclimatic can be reconstructed with a very high temporal resolution from continental deposits.

Acknowledgements

We would like to thank Heidelberger Zement AG for permitting to work in their quarries. Funding was provided by the Deutsche Forschungsgemeinschaft (HA 2193/2-1), the CEA, the CNRS, the EC Environment Program BIMACEL (No. EV5V-CT93-0298), the CNRS PNEDC and the VARIENTE. We thank S. Lindauer for sample preparation and G.A. Wagner for providing the possibility of carrying out OSL dating at the Forschungsstelle Archäometrie in Heidelberg. The UMS 2004 and Maurice Arnold are acknowledged for AMS ^{14}C measurements on graphite targets; Contribution ISEM2002-035.

References

Aitken, M.J., Xie, J., 1992. Optical dating using infrared diodes: young samples. Quaternary Science Reviews 11, 147–152.

Antoine, P., Rousseau, D.-D., Lautridou, J.-P., Hatté, C., 1999. Last interglacial–glacial climatic cycle in loess-palaeosol successions of northwestern France. Boreas 28, 551–563.

Antoine, P., Rousseau, D.-D., Zöller, L., Lang, A., Munaut, A.V., Hatté, C., Fontugne, M., 2001. High-resolution record of the last interglacial–glacial cycle in the Nußloch loess-palaeosol sequences, Upper Rhine Area, Germany. Quaternary International 76, 211–229.

Felix, C., Singhvi, A.K., 1997. Study of non-linear luminescence dose growth curves for the estimation of paleodose in luminescence dating: results of Monte Carlo simulation. Radiation Measurements 27, 599–609.

Frechen, M., 1999. Upper Pleistocene loess stratigraphy in Southern Germany. Quaternary Geochronology 18, 243–269.

Goodfriend, G.A., Hood, D.G., 1983. Carbon isotope analysis of land snail shells: implications for carbon sources and radiocarbon dating. Radiocarbon 25, 810–830.

Hatté, C., Pessenda, L.C., Lang, A., Paterne, M., 2001a. Development of an accurate and reliable ^{14}C-chronology for loess sequences. Application to the loess sequence of Nußloch (Rhine Valley, Germany). Radiocarbon 43, 611–618.

Hatté, C., Morvan, J., Noury, C., Paterne, M., 2001b. Is classical acid–alkali–acid treatment responsible for contamination? An alternative proposition. Radiocarbon 43, 177–182.

Hatté, C., Antoine, P., Fontugne, M., Lang, A., Rousseau, D.D., Zöller, L., 2001c. $\delta^{13}C$ of loess organic matter as a potential proxy for paleoprecipitation reconstruction. Quaternary Research 55, 33–38.

Huntley, D.J., Lamothe, M., 2001. Ubiquity of anomalous fading in K-feldspars and the measurement and correction for it in optical dating. Canadian Journal of Earth Sciences 38, 1093–1106.

Huntley, D.J., Godfrey-Smith, D.I., Thewalt, M.L.W., 1985. Optical dating of sediments. Nature 313, 105–107.

Hütt, G., Jaek, I., Tchonka, J., 1988. Optical dating: K-feldspars optical response stimulation spectra. Quaternary Science Reviews 7, 381–385.

Kitagawa, H., van der Plicht, J., 1998. Atmospheric radiocarbon calibration to 45,000 yr B.P.: late glacial fluctuations and cosmogenic isotope production. Science 279, 1187–1190.

Krbetschek, M., Rieser, U., 1995. Luminescence spectra of alkalifeldspars and plagioclases. Radiation Measurement 24, 473–477.

Lamothe, M., Auclair, M., 1997. Assessing the datability of young sediments by IRSL using an intrinsic laboratory protocol. Radiation Measurement 27, 107–117.

Lang, A., Wagner, G.A., 1997. Infrared stimulated luminescence dating of Holocene colluvial sediments using the 410 nm emission. Quaternary Science Reviews 16, 393–396.

Lang, A., Lindauer, S., Kuhn, R., Wagner, G.A., 1996. Procedures used for optically and infrared stimulated luminescence dating of sediments in Heidelberg. Ancient TL 14, 7–11.

Roberts, H., Zhou, L.-P., Wintle, A., Zőller, L., in press. Dating loess. In: Stokes, S. (Ed.), Luminescence Dating. Springer, Berlin.

Rousseau, D.-D., Antoine, P., Hatté, C., Lang, A., Zöller, L., Fontugne, M., Othman, B.D., Luck, J.-M., Moine, O., Labonne, M., Bentaleb, I., Jolly, D., 2002. Abrupt millennial climatic terrestrial changes from Nußloch (Germany) Upper Weichselian eolian records during the Last Glaciation? Quaternary Science Reviews 21, 1577–1582.

Stokes, S., Armitage, S., Singhvi, A., in press. Luminescence dating, desert sedimentary environments. In: Stokes, S. (Ed.), Luminescence Dating. Springer, Berlin.

Stuiver, M., Reimer, P.J., 1993. Extended 14C data base and revised calib 3.0 14C age calibration program. Radiocarbon 35, 215–230.

Wallinga, J., Lang, A., in press. Beyond aeolian sediments: applications of luminescence dating in fluvial, colluvial and other sedimentary environments. In: Stokes, S. (Ed.), Luminescence Dating. Springer, Berlin.

Zöller, L., Stremme, H.E., Wagner, G.A., 1988. Thermolumineszenz-Datierung an Löß-Paläoboden-Sequenzen von Nieder-, Mittel- und Oberrhein. Chemical Geology (Isotope Geoscience Section) 73, 39–62.